Chinese Physics Letters **42**, 047302 (2025) **Express Letter**

Quantum Metric, Topology and Second Harmonic Generation

En Wang(王恩)[1,2], Yaxian Wang(王亚娴)[1,2*], and Sheng Meng(孟胜)[1,2,3*]

[1]*Beijing National Laboratory for Condensed Matter Physics and Institute of Physics, Chinese Academy of Sciences, Beijing 100190, China*
[2]*School of Physical Sciences, University of Chinese Academy of Sciences, Beijing 100190, China*
[3]*Songshan Lake Materials Laboratory, Dongguan 523808, China*

(Received 18 January 2025; accepted manuscript online 21 March 2025)

The quantum metric manifested as the Riemannian metric in the parameter space of Bloch bands, characterizes the topology and geometry of quantum states. The second harmonic generation (SHG), as one of the fundamental nonlinear optical responses that links geometry of optical transitions to physical observables, despite being widely studied in various materials, its relation to quantum metric, especially in the dynamical regime, stays obscure. Here, we investigate the SHG within the Keldysh formalism and resolve the contributions from quantum metric. Using a Haldane model, we simulate the dynamic photocurrent, revealing a significant enhancement of SHG in the transparent region, i.e., for below-gap photon energies. Further, we show that such enhancement originates from the non-Hermitian nature of its complex band structure and quantum tunneling near the exceptional points. Such low-energy-photon SHG signals are highly sensitive to the topological phase transition, quantifying the quantum volume effect. Our work elucidates the physical origin of quantum metric contributed SHG and its relation with topology, providing an alternative route to probe the ultrafast topological phase transition in magnetic insulators.

DOI: 10.1088/0256-307X/42/4/047302 CSTR: 32039.14.0256-307X.42.4.047302

Nonlinear optical response (NLOR), particularly second harmonic generation (SHG), is a fundamental and universal nonlinear optical phenomenon in quantum materials, where geometric quantities are embedded.[1–15] The geometry of Bloch wavefunction is characterized by the quantum geometric tensor (QGT),[16–23] with the real part being the quantum metric (QM),[24–43] also referred to as Riemannian metric of Bloch states, and the imaginary part corresponds to the Berry curvature (BC).[29,30,44] The geometrical description of NLOR can also be extended to include many-body interaction.[45,46] Typically, perturbative methods, including both semiconductor Bloch equations[4,5,47–49] and the diagrammatic techniques[50,51] have been employed to analytically derive the SHG susceptibility, providing profound insights into the SHG signal and its relation to the geometric properties from both theoretical[32,52,53] and experimental[54–56] perspective. However, little attention has been paid to the dynamics of SHG. For instance, when the photon energy is high enough to excite an electron from valence bands (VB) to conduction bands (CB) via absorption of photons,[29] the SHG dynamics is naturally related to the shift vector (SV), i.e., the position change of Wannier center during photoexcitation. In the transparent region, typical two-photon resonant absorption is not met but the in-gap optical rectification could still exist.[57–60] The comprehensive study of such excitation processes, such as their distinctive symmetry and dynamics, especially the effects of quantum metric, remains elusive.

In this Letter, we employ the Keldysh formalism[61–66] to simulate SHG dynamics, which goes beyond the linear response description. In order to quantitatively illustrate the role of quantum metric, we present a rigorous investigation on the SHG dynamics using a Haldane model.[67,68] The SHG is computed from the photocurrent in the time domain by numerically solving the time-dependent Schrödinger equation (TDSE). More importantly, we distinguish contributions from the QGT and the SV via the evolution of SHG patterns upon tuning photon energy. We further reveal a significant quantum-metric enhanced SHG for below-gap photons due to the non-Hermitian nature of SHG dynamics. In light of these results, we discuss the possibility of utilizing SHG as a probe for ultrafast topological phase transitions. Our work highlights a previously overlooked dynamical perspective of SHG and its correspondence to non-Hermitian dynamics under laser illumination,[69–71] offering new understandings of NLOR of quantum materials.

Decomposition of SHG Dynamics. We start from a time-dependent Hamiltonian with a light field in the length gauge in the following form (atomic unit is adopted throughout the text unless specified otherwise):

$$\hat{H}(t) = \hat{H}_0 - \hat{\boldsymbol{r}} \cdot \boldsymbol{E}(t), \tag{1}$$

where $\hat{H}_0$ is the unperturbed Hamiltonian, $\hat{\boldsymbol{r}}$ the posi-

*Corresponding author. Email: yaxianw@iphy.ac.cn; smeng@iphy.ac.cn
© 2025 Chinese Physical Society and IOP Publishing Ltd. All rights, including for text and data mining, AI training, and similar technologies, are reserved.

tion operator, and $\boldsymbol{E}(t)$ is the electrical component of the light field. The corresponding vector potential is $\boldsymbol{A}(t) = -\int_{-\infty}^{t} \mathrm{d}t' \boldsymbol{E}(t')$.[72,73] The quasi-momentum is now $\boldsymbol{K} = \boldsymbol{k} - \boldsymbol{A}(t)$, and the associated Brillouin zone is referred to as the shifted Brillouin zone (SBZ) and denoted as $\overline{\mathrm{BZ}} = \mathrm{BZ} - \boldsymbol{A}(t)$. The time evolution is modeled using the two level density matrix equations.

In practice, the SHG signal can be derived from the expectation value of the current density operator $\hat{\boldsymbol{J}}_{\boldsymbol{k}} = -\hat{\boldsymbol{v}}_{\boldsymbol{k}} = -\nabla_{\boldsymbol{k}}\hat{H}_{\boldsymbol{k}}$, with $\hat{H}_{\boldsymbol{k}} = \mathrm{e}^{\mathrm{i}\boldsymbol{k}\cdot\hat{\boldsymbol{r}}}\hat{H}_0\mathrm{e}^{-\mathrm{i}\boldsymbol{k}\cdot\hat{\boldsymbol{r}}}$ and $\hat{\boldsymbol{v}}_{\boldsymbol{k}}$ is the velocity operator in the reciprocal space. Mathematically, SHG computed in this way has incorporated both $\boldsymbol{j}_{\mathrm{D}}$ and $\boldsymbol{j}_{\mathrm{OD}}$ currents, which emerge from the diagonal (D) and off-diagonal (OD) elements of $\hat{\boldsymbol{J}}_{\boldsymbol{k}}$ respectively. The current $\boldsymbol{j}_{\mathrm{OD}}$ can be further decomposed to SV term $\boldsymbol{j}_{\mathrm{SV}}$ and QGT term $\boldsymbol{j}_{\mathrm{QGT}}$ from distinct physical origins (see Supplementary Material (SM)[74] for detailed derivation). We will discuss these three components below to provide the basis for this article.

The current $\boldsymbol{j}_{\mathrm{D}}$ can be expressed as follows:

$$j^{\mu}_{\mathrm{D}}(t) = -\sum_{m=1,2}\int_{\boldsymbol{K}} v^{\mu}_{mm}(\boldsymbol{K}_t)n_m(\boldsymbol{K},t), \tag{2}$$

from which we can further transform the current into the frequency domain via $\boldsymbol{j}(\omega) = \int \boldsymbol{j}(t)\mathrm{e}^{-\mathrm{i}\omega t}\mathrm{d}t$. Here $\int_{\boldsymbol{K}} \equiv \frac{1}{(2\pi)^3}\int_{\overline{\mathrm{BZ}}}\mathrm{d}\boldsymbol{K}$ denotes the integration over SBZ. Note that here we have substituted the integration variable from $\boldsymbol{k}$ to $\boldsymbol{K}$ and have used notation $\boldsymbol{K}_\tau = \boldsymbol{K} + \boldsymbol{A}(\tau)$ for short with $\boldsymbol{K}_t \equiv \boldsymbol{k}$. μ denotes the Cartesian coordinate of photocurrent, while $m = 1, 2$ is the band index of CB and VB respectively. v^{μ}_{mm} is the diagonal element of velocity operator, which is also the group velocity of band m and n_m is the occupation of each band, which is also the diagonal element of density matrix. The off-diagonal element is denoted as $\pi(\boldsymbol{K}, t)$. Given that the total number of electron is fixed, current in Eq. (2) is related to the carrier density n_m and group velocity difference $\boldsymbol{\Delta} = \boldsymbol{v}_{11} - \boldsymbol{v}_{22}$ between the CB and the VB, as illustrated in Fig. 1(a). As the current induced by carrier movement is negligible in our numerical calculations (evidenced by Fig. S1 in Supplementary Material), we exclude this component from subsequent analyses.

The current $\boldsymbol{j}_{\mathrm{OD}}(\omega)$ has the following form assuming the low excitation condition:

$$\begin{aligned} j^{\mu}_{\mathrm{OD}}(\omega) =& -\int_{-\infty}^{\infty}\mathrm{d}t\int_{\boldsymbol{K}} v^{\mu}_{12}(\boldsymbol{K}_t)\pi(\boldsymbol{K},t)\mathrm{e}^{\mathrm{i}S(\boldsymbol{K},t)-\mathrm{i}\omega t} + \mathrm{c.c.} \\ =& \mathrm{i}\int_{-\infty}^{\infty}\mathrm{d}t\int_{\boldsymbol{K}} v^{\mu}_{12}(\boldsymbol{K}_t)\int_{-\infty}^{t}\mathrm{d}t'\boldsymbol{E}(t')\cdot\boldsymbol{d}^{*}(\boldsymbol{K}_{t'}) \\ &\times \mathrm{e}^{\mathrm{i}S(\boldsymbol{K},t,t')-\mathrm{i}\omega t} + \mathrm{c.c.}. \end{aligned} \tag{3}$$

Here $\boldsymbol{d}(\boldsymbol{k}) \equiv \boldsymbol{r}_{12}(\boldsymbol{k})$ is the off-diagonal matrix element of position operator $\hat{\boldsymbol{r}}$. The phase term $S(\boldsymbol{K}, t, t')$ which describes the creation and annihilation of an electron-hole pair is

$$S(\boldsymbol{K},t,t') = \int_{t'}^{t}(\varepsilon_{\mathrm{g}}(\boldsymbol{K}_{t''}) - \boldsymbol{E}(t'')\cdot\boldsymbol{r}_{\mathrm{g}}(\boldsymbol{K}_{t''}))\,\mathrm{d}t'', \tag{4}$$

where $\varepsilon_{\mathrm{g}} = \varepsilon_1 - \varepsilon_2$ is the energy difference and $\boldsymbol{r}_{\mathrm{g}} = \boldsymbol{r}_1 - \boldsymbol{r}_2$ is the position difference of CB and VB.

To obtain the explicit origins of SHG dynamics, we utilize the covariant derivative $\boldsymbol{\mathcal{D}} = -\mathrm{i}\hat{\boldsymbol{r}}$[50,75] to expand Eq. (3). After expansion, we get the photocurrent with second harmonic processes that can be decomposed into the SV term and the QGT term,

$$\begin{aligned} j^{\mu}_{\mathrm{SV}}(\omega) =& \mathrm{i}\int_{-\infty}^{\infty}\mathrm{d}t\int_{-\infty}^{t}\mathrm{d}t'\int_{\boldsymbol{K}}\mathrm{i}\varepsilon_{\mathrm{g}}(\boldsymbol{K}_t) \\ &\times\{[\boldsymbol{A}(t)\cdot\boldsymbol{\mathcal{D}}d_{\mu}(\boldsymbol{K})][\boldsymbol{E}(t')\cdot\boldsymbol{d}^{*}(\boldsymbol{K}_{t'})] \\ &+ d_{\mu}(\boldsymbol{K}_t)\boldsymbol{A}(t')\boldsymbol{E}(t'):\boldsymbol{\mathcal{D}}\boldsymbol{d}^{*}(\boldsymbol{K})\} \\ &\times \mathrm{e}^{\mathrm{i}S(\boldsymbol{K},t,t')-\mathrm{i}\omega t} + \mathrm{c.c.}. \end{aligned} \tag{5}$$

Here we use double dot product to simplify the formula and the SV contribution emerges from the covariant derivative over the dipole operator $\mathcal{D}_\alpha d_\mu = -\mathrm{i}d_\mu R^{\mu,\alpha}_{12}$[50] with $R^{\mu,\alpha}_{12}$ being the shift vector, illustrated in Fig. 1(b). On the other hand, the QGT contribution, depicted in Fig. 1(c), can be obtained from the cross product with the following form:

$$\begin{aligned} j^{\mu}_{\mathrm{QGT}}(\omega) =& \mathrm{i}\int_{-\infty}^{\infty}\mathrm{d}t\int_{-\infty}^{t}\mathrm{d}t'\int_{\boldsymbol{K}}\mathrm{i}\boldsymbol{A}(t)\cdot\boldsymbol{\Delta}(\boldsymbol{K}) \\ &\times d_{\mu}(\boldsymbol{K}_t)[\boldsymbol{E}(t')\cdot\boldsymbol{d}^{*}(\boldsymbol{K}_{t'})]\mathrm{e}^{\mathrm{i}S(\boldsymbol{K},t,t')-\mathrm{i}\omega t} + \mathrm{c.c.}. \end{aligned} \tag{6}$$

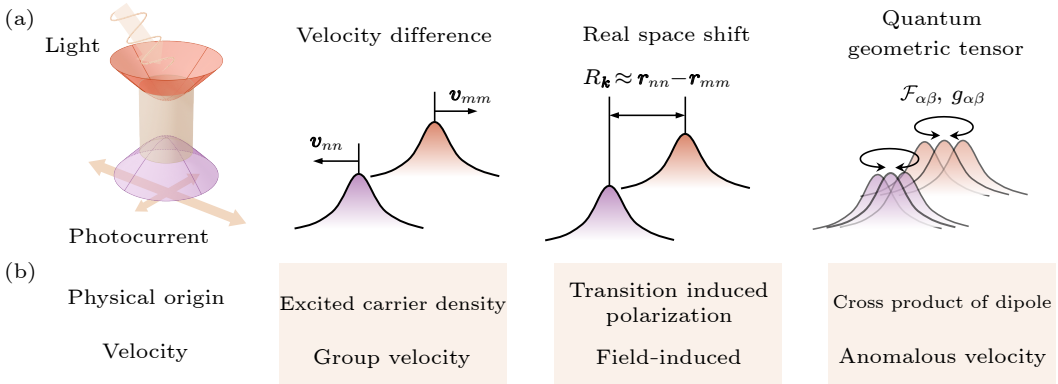

Fig. 1. Illustration of SHG mechanism. Despite the contribution from the group velocity of excited carriers, SHG contains two fundamental geometric contributions - the shift vector (SV) emerging from the connection term and quantum geometric tensor (QGT) manifesting metric term within the manifold of Bloch electrons. We note that the SV contribution arises from direct excitation when twice the photon energy exceeds the gap. The QGT contribution is non-zero only when time-reversal symmetry is broken.

We note that the QGT-contributed SHG susceptibility is an excitation effect corresponding to the anomalous velocity of the wave packet.[6,44] Such separation is also valid in the perturbation formulation,[49,50] but the decomposition of general SHG susceptibility requires careful treatment of the time-reversal symmetry since the QGT term only exists in the time-reversal symmetry breaking systems.

SHG Pattern of a Haldane Model. We now employ a standard Haldane model to investigate the SHG signal from *real-time* calculation. Specifically, we solve the TDSE with Hamiltonian in velocity gauge

$$\hat{H}'(t) = \hat{H}_0[\boldsymbol{k} - \boldsymbol{A}(t)], \tag{7}$$

which is equivalent to Eq. (1) in length gauge[52,76,77] (see computational details in SM[74] Section S2).

The Haldane Hamiltonian reads

$$H_0(\boldsymbol{k}) = B_{0,\boldsymbol{k}}\sigma_0 + \boldsymbol{B}_{\boldsymbol{k}} \cdot \boldsymbol{\sigma}, \tag{8}$$

where we simplify the electron hopping as a pseudomagnetic field with $B_{0,\boldsymbol{k}} = 2t_2 \cos\phi \sum_i \cos(\boldsymbol{k}\cdot\boldsymbol{b}_i)$ and $\boldsymbol{B}_{\boldsymbol{k}} = (B_{1,\boldsymbol{k}}, B_{2,\boldsymbol{k}}, B_{3,\boldsymbol{k}})$ with

$$\begin{aligned} &B_{1,\boldsymbol{k}} = t_1 \sum_i \cos(\boldsymbol{k}\cdot\boldsymbol{a}_i), \quad B_{2,\boldsymbol{k}} = t_1 \sum_i \sin(\boldsymbol{k}\cdot\boldsymbol{a}_i), \\ &B_{3,\boldsymbol{k}} = M + 2t_2 \sin\phi \sum_i \sin(\boldsymbol{k}\cdot\boldsymbol{b}_i). \end{aligned} \tag{9}$$

Here $\boldsymbol{a}_i$ are the lattice vectors of nearest-neighbor (NN) hopping and $\boldsymbol{b}_1 = \boldsymbol{a}_2 - \boldsymbol{a}_3$, $\boldsymbol{b}_2 = \boldsymbol{a}_3 - \boldsymbol{a}_1$ and $\boldsymbol{b}_3 = \boldsymbol{a}_1 - \boldsymbol{a}_2$ are the lattice vectors of next-to-nearest-neighbor (NNN) hopping in honeycomb lattice, t_1 and $t_2 e^{i\phi}$ are the corresponding NN and NNN hopping and M is the mass term [Fig. 2(a)]. For $|M| < |3\sqrt{3}t_2 \sin\phi|$, the system is topologically nontrivial. We emphasize that the electron accumulated phase $\phi \neq 0$ through NNN hopping will dramatically affect the SHG, which we will come back to later.

As seen in Fig. 2(b), there is a noticeable change in the SHG pattern with decreasing photon energy due to interplay between SV and QGT contributions. Such interplay is indicated by the phase factor $e^{i\alpha}$ [Fig. 2(c)]. The magnetic 2D point group of Haldane model is $3m'1$, including a three-fold rotation operation $\mathcal{C}_{3z}$, and a combined operation $\mathcal{M}_y\mathcal{T}$ ($\mathcal{M}_y$ is mirror operation that reverses the y axis and $\mathcal{T}$ is time-reversal operation). Constrained by symmetry of Haldane model,[7,78] the BC term in the QGT component of SHG vanishes and the QM term survives, which is also remarkably enhanced in the transparent region with low photon energy ω_L.

Here we present the details of resolving the QGT component in SHG. Since the QGT term in Eq. (6) is weighted with group velocity difference $\boldsymbol{\Delta}(\boldsymbol{K})$, it can be decomposed into $\mathcal{T}$-odd component from quantum metric $g_{\alpha\beta}$ and $\mathcal{T}$-even component from Berry curvature $\mathcal{F}_{\alpha\beta}$. For the $\mathcal{T}$-even component, we consider only the point group symmetry operations $\mathcal{C}_{3z}$ and $\mathcal{M}_y$, which yields nonzero SHG susceptibility:

$$\chi_{xxx} = -\chi_{xyy} = -\chi_{yxy} = -\chi_{yyx} = \chi_{\text{even}}. \tag{10}$$

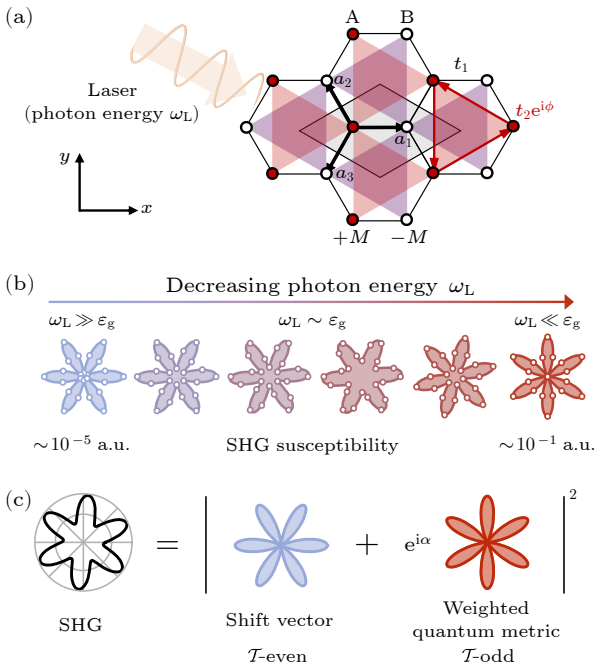

Fig. 2. SHG pattern of a Haldane model. (a) Illustration of the Haldane model for a honeycomb lattice. (b) The simulated SHG pattern with decreasing photon energy in Haldane model with parameters $\phi = \pi/6$, $t_1 = -1$, $t_2 = 0.15$ and $M = 0.2$ in atomic unit. Such evolution of symmetry highlights an obvious change of underlying physical mechanism, accompanied by great enhancement of SHG at low-photon-energy regime. (c) The physical origin of SHG in Haldane model is decomposed to the time-reversal operation $\mathcal{T}$-even shift vector (SV), and the $\mathcal{T}$-odd weighted quantum metric (real part of QGT) parts.

For the $\mathcal{T}$-odd part, operation $\mathcal{T}$ will introduce an additional minus sign. Thus the effective operation for $\mathcal{M}_y\mathcal{T}$ becomes $\mathcal{M}_y\mathcal{P}$. Such distinct symmetry results in SHG susceptibility differing from Eq. (10) which reads

$$\chi_{yxx} = -\chi_{yyy} = \chi_{xxy} = \chi_{xyx} = \chi_{\text{odd}}. \tag{11}$$

It is worth noting that since SV is time-reversal invariant, the nonzero SHG susceptibility of SV term also has the form given in Eq. (10).

For a generic two-dimensional magnetic insulator, its symmetry is manifested through the magnetic point group (MPG). Given that type-III MPG contains anti-symmetry versions of half of the symmetry operations, such operations constrain various components of QGT, thereby revealing distinct geometric quantities. Due to the antisymmetric property of BC, the nonzero SHG components from BC only exist for MPG m'. The QM term, on the other hand, exists for m', $m'm2'$, $3m'1$, $31m'$, $6'$, and $6'mm'$ (see the full table of nonzero components of SHG susceptibility in SM[74] Section S4).

Metric Enhanced SHG via Non-Hermitian Nature. To further explore the key ingredient of SHG, especially the SHG contributed by QGT in the transparent region, we utilize saddle point analysis to Eqs. (5) and (6). For monochromatic light fields $\boldsymbol{E}(t) = \boldsymbol{E}_0 e^{i\omega_L t}$ + c.c. with photon energy ω_L, the dynamics are governed by sad-

dle point conditions (SPCs) of the semiclassical action $\mathcal{S}$ displayed in final expression with form of phase factor $\exp(\mathrm{i}\mathcal{S})$.[79] The QGT component is associated with action $\mathcal{S} = S(\boldsymbol{K}, t, t') - (\omega - \omega_\mathrm{L})t - \omega_\mathrm{L}t'$. The SPCs are

$$\boldsymbol{\mathcal{D}}S = \Delta\boldsymbol{r} - \Delta\boldsymbol{R} = 0, \tag{12a}$$

$$\frac{\mathrm{d}S}{\mathrm{d}t'} = \varepsilon_\mathrm{g}(\boldsymbol{K}_{t'}) = \omega_\mathrm{L}, \tag{12b}$$

$$\frac{\mathrm{d}S}{\mathrm{d}t} = \varepsilon_\mathrm{g}(\boldsymbol{K}_t) = \omega - \omega_\mathrm{L}. \tag{12c}$$

Here we ignore the dipole energy of the electron–hole pair (see SM[74] Section S1 for further details and SPCs of SV terms). Moreover, $\Delta\boldsymbol{R} = \boldsymbol{R}^\mu_{12}(\boldsymbol{K}_t) - \boldsymbol{R}^\mu_{12}(\boldsymbol{K}_{t'})$ is the difference of SV and $\Delta\boldsymbol{r} \approx \int_{t'}^{t} \mathrm{d}t''\boldsymbol{\Delta}(\boldsymbol{K}_{t''})$.

As for photon energy $\omega_\mathrm{L} \geq \varepsilon_\mathrm{g}$, one of the SPCs in Eq. (12b) corresponds to the *direct excitation* of electron with the absorption of a photon $\varepsilon_\mathrm{g}(\boldsymbol{K}_{t'}) = \omega_\mathrm{L}$ at time t'. The other SPCs in Eq. (12c) correspond to the absorption of another photon with energy ω_L and the subsequent emission of a photon with energy $\omega = 2\omega_\mathrm{L}$ at time t. In the transparent region with $\omega_\mathrm{L} < \varepsilon_\mathrm{g}$, the SPCs in Eqs. (12b) and (12c) have no real solution. Therefore, it is necessary to extend this analysis to the complex time plane, where the transparent region dynamics can naturally manifest as *quantum tunneling*. The complex solutions also elucidate the direct contribution of SHG from the edge states.[80] We note that one can introduce relaxation time τ and replace $\omega_\mathrm{L} \to \omega_\mathrm{L} + \mathrm{i}/\tau$ in SPCs to account for the relaxation effect. For our purpose, under the condition of frequencies above the width of the Drude peak $\omega_\mathrm{L}\tau \gg 1$, the relaxation effect of QM contributed SHG is negligible. In the absence of the assumption $\omega_\mathrm{L}\tau \gg 1$, the relaxation effect would suppress the QM contributed SHG intensity.

Following Refs. [81,82], the Hermitian band structure of our Haldane model displays finite gap [Fig. 3(a)], while the complex band structure reveals gap closing points marked with arrows as plotted in Fig. 3(b). The color represents $\mathrm{Re}\,[\varepsilon_\mathrm{g}(\boldsymbol{k})]$ and the dashed line depicts the real axis with $\boldsymbol{k} = (\mathrm{Re}\,k, 0)$. Near K and K' points, the massive Dirac model $H_\mathrm{D} = k\sigma_x + M_\mathrm{eff}\sigma_z$ with complex k can serve as an effective model, with eigenvalues $\varepsilon_\pm = \pm\sqrt{k^2 + M_\mathrm{eff}^2}$. The detailed complex band structure of H_D is shown in Fig. 3(c). Within $M_\mathrm{eff} \neq 0$, the energy spectrum shows an explicit gap with solid purple line. When the complexation is applied to k, H_D becomes non-Hermitian, where the gap closes at $k_0 = \mathrm{i}M_\mathrm{eff}$, i.e., the exceptional point (EP) of the non-Hermitian system.

For low-photon-energy excitation in the transparent region, solutions of SPCs concentrate near EPs, greatly enhancing the QGT contribution. For a two-band system, QGT scales as $1/\varepsilon_\mathrm{g}^2$, transforming to $1/\omega_\mathrm{L}^2$ upon inserting the solutions of SPCs. This demonstrates the QGT term, i.e., QM term in Haldane model is enhanced by lowering the photon energy in the transparent region. Conversely, the SV vanishes for degenerate states (See SM[74] Section S1 for detailed analysis).

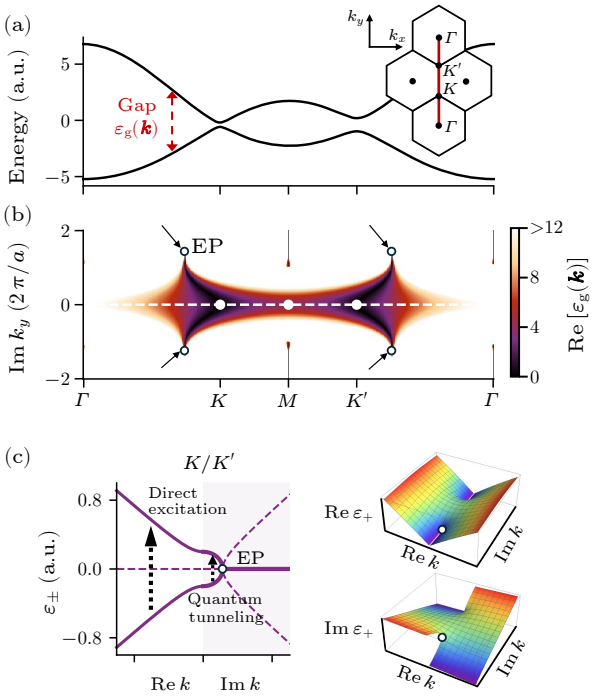

Fig. 3. Non-Hermitian nature and dynamical behavior of SHG in the transparent region. (a) The Hermitian band structure of Haldane model with parameters $\phi = \pi/6$, $t_1 = -1$, $t_2 = 0.15$ and $M = 0.2$ along the high-symmetry path $\Gamma K M K' \Gamma$. (b) The energy gap when replacing $\boldsymbol{k}$ with the complex variable. The dashed white line represents $\mathrm{Im}\,k \equiv 0$ and the vertical axis shows the imaginary part $\mathrm{Im}\,k$. The colormap represents the real part of energy gap $\mathrm{Re}\,[\varepsilon_\mathrm{g}]$ and the gap closing points are marked with arrows. (c) The complex band structure of the massive Dirac model. In the left panel, the solid lines represent $\mathrm{Re}\,\varepsilon_\pm$ and the dashed lines represent $\mathrm{Im}\,\varepsilon_\pm$. The right panel displays the full complex spectrum of ε_+.

SHG During Topological Transition. We further investigate the SHG feature along the topological phase transition. For a Chern insulator, the quantum volume vol_g is defined as[18]

$$\mathrm{vol}_g = \int_{\boldsymbol{k}} \sqrt{\det(g_{\alpha\beta})} = \int_{\boldsymbol{k}} \sqrt{g_{xx}g_{yy} - g_{xy}^2} \geq \pi|\mathcal{C}|, \tag{13}$$

which is the integral of quantum metric $g_{\alpha\beta}$ and gives a good estimate of the topology usually given by the Chern number $\mathcal{C}$. Consequently, the magnitude of QM-contributed SHG susceptibility χ_QM could be estimated through the following relation after separating the group velocity difference $\boldsymbol{\Delta}$ and the QM in the integral (see details in SM[74] Section S5),

$$|\chi_\mathrm{QM}| \sim \mathrm{vol}_g \cdot \int_{\boldsymbol{k}} |\boldsymbol{\Delta}| \geq \pi|\mathcal{C}| \int_{\boldsymbol{k}} |\boldsymbol{\Delta}|. \tag{14}$$

For an arbitrarily given Haldane model, the time-dependent photocurrent and the corresponding SHG intensity are shown in Fig. 4(a). By varying the photon energy and the phase factor ϕ that determines the topology of Haldane model, we obtain the SHG spectral response within the full two-dimensional parameter space, shown in Fig. 4(b). In this analysis, we use averaged band gap

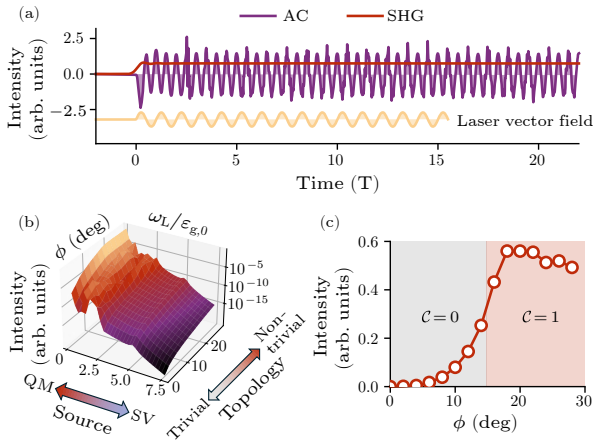

Fig. 4. (a) The time-dependent alternating photocurrent (AC) and the corresponding SHG intensity from Fourier transformation. (b) The SHG spectrum with different photon energy ω and phase factor ϕ. (c) The SHG spectrum at photon energy $\omega_L/\varepsilon_{g,0} = 1/4$ and the corresponding Chern number with dependence on ϕ, highlighting a phase transition behavior.

$\varepsilon_{g,0} = 2M$ as the reference scale for characterizing photon energy ω_L. A typical representation in the transparent region with photon energy $\omega_L/\varepsilon_{g,0} = 1/4$ is further visualized in Fig. 4(c). The topological phase transition occurs at $\phi_0 = \arcsin(M/3\sqrt{3}t_2)$, where a great enhancement for the SHG intensity can be clearly seen, indicating SHG as a unique probe for topological phase transitions. We note that such topological enhancement persists with high photon energy, when the shift vector's contribution exhibits comparable magnitude to the quantum metric.

Summary. We present a comprehensive investigation of SHG dynamics and resolve the three components of SHG in the Keldysh formulation, with particular highlights on the quantum geometric tensor contribution. Using the Haldane model, we compute the dynamical photocurrent and SHG, and observe the quantum metric enhanced signal in the transparent region. Furthermore, we uncover the connection between the SHG response and non-Hermitian physics, offering new insights into the non-Hermitian nature of SHG. The antiferromagnetic monolayer $MnPSe_3$ $(6'mm')$[83] and gate-tunable Chern insulators in moiré systems,[84] both exhibiting the required symmetry, serve as promising platforms for exploring the quantum metric effects and topology-enhanced SHG detected by mid-infrared light.[85] Recently, there has also been loss-enhanced magneto-optical effect reported.[86]

The SHG susceptibility shows a direct connection to the Chern number through quantum volume, establishing a link between topological invariants and the NLOR. While our method focuses on the underlying physics and neglects the multiband geometric quantities, the potential contribution arising from other bands requires further study. Our results advance our understanding of topology-enhanced light–matter interactions and suggest SHG as a promising probe for topological phase transitions and geometry in quantum materials.

Acknowledgements. This work is supported by National Natural Science Foundation of China (Grant Nos. 12025407, 12474246, and 12450401), the National Key Research and Development Program of China (Grant No. 2021YFA1400201), and the Chinese Academy of Sciences (Grant Nos. YSBR-047 and XDB33030100).

References

[1] Nagaosa N 2022 *Ann. Phys.* **447** 169146
[2] Ma Q, Kumar R K, Xu S Y, Koppens F H L, and Song J C W 2023 *Nat. Rev. Phys.* **5** 170
[3] Boyd R W 2019 *Nonlinear Optics* 4th edn (Academic Press)
[4] Aversa C and Sipe J E 1995 *Phys. Rev. B* **52** 14636
[5] Sipe J E and Shkrebtii A I 2000 *Phys. Rev. B* **61** 5337
[6] Fregoso B M 2019 *Phys. Rev. B* **100** 064301
[7] Xiao R C, Shao D F, Gan W, Wang H W, Han H, Sheng Z G, Zhang C J, Jiang H, and Li H 2023 *npj Quantum Mater.* **8** 62
[8] Lin K Q, Bange S, and Lupton J M 2019 *Nat. Phys.* **15** 242
[9] Zhang X, Carbin T, Culver A B, Du K, Wang K, Cheong S W, Roy R, and Kogar A 2024 *Nat. Mater.* **23** 1
[10] Wang C, Zhao S B, Guo X M, Ren X G, Gu B L, Xu Y, and Duan W H 2019 *New J. Phys.* **21** 093001
[11] Wang C, Liu X Y, Kang L, Gu B L, Xu Y, and Duan W H 2017 *Phys. Rev. B* **96** 115147
[12] Lerner G, Neufeld O, Hareli L, Shoulga G, Bordo E, Fleischer A, Podolsky D, Bahabad A, and Cohen O 2023 *Sci. Adv.* **9** eade0953
[13] Zhou H, Xiao R C, Zhang S H, Gan W, Han H, Zhao H M, Lu W J, Zhang C J, Sun Y P, Li H, and Shao D F 2024 *Phys. Rev. Lett.* **133** 236903
[14] Cook A M, Fregoso B M, De Juan F, Coh S, and Moore J E 2017 *Nat. Commun.* **8** 14176
[15] Bhalla P, Das K, Culcer D, and Agarwal A 2022 *Phys. Rev. Lett.* **129** 227401
[16] Törmä P 2023 *Phys. Rev. Lett.* **131** 240001
[17] Cheng R 2013 arXiv:1012.1337 [quant-ph]
[18] Ozawa T and Mera B 2021 *Phys. Rev. B* **104** 045103
[19] Neupert T, Chamon C, and Mudry C 2013 *Phys. Rev. B* **87** 245103
[20] Gianfrate A, Bleu O, Dominici L, Ardizzone V, De Giorgi M, Ballarini D, Lerario G, West K W, Pfeiffer L N, Solnyshkov D D, Sanvitto D, and Malpuech G 2020 *Nature* **578** 381
[21] Provost J P and Vallee G 1980 *Commun. Math. Phys.* **76** 289
[22] Yu J B, Herzog-Arbeitman J, and Bernevig B A 2024 arXiv:2501.00100 [cond-mat.mes-hall]
[23] Yu J B, Bernevig B A, Queiroz R, Rossi E, Törmä P, and Yang B J 2024 arXiv:2501.00098
[24] Higuchi K, Sakamoto W, and Higuchi M 2024 *Phys. Rev. B* **110** 205131
[25] Uzan-Narovlansky A J, Faeyrman L, Brown G G, Shames S, Narovlansky V, Xiao J W, Arusi-Parpar T, Kneller O, Bruner B D, Smirnova O, Silva R E F, Yan B H, Jiménez-Galán Á, Ivanov M, and Dudovich N 2024 *Nature* **626** 66
[26] Kang M G, Kim S J, Qian Y T, Neves P M, Ye L, Jung J S, Puntel D, Mazzola F, Fang S A, Jozwiak C, Bostwick A, Rotenberg E, Fuji J, Vobornik I, Park J H, Checkelsky J G, Yang B J, and Comin R 2025 *Nat. Phys.* **21** 110
[27] Du Z Z, Lu H Z, and Xie X C 2021 *Nat. Rev. Phys.* **3** 744
[28] Wang C, Gao Y, and Xiao D 2021 *Phys. Rev. Lett.* **127** 277201

[29] Morimoto T and Nagaosa N 2016 *Sci. Adv.* **2** e1501524
[30] Sodemann I and Fu L 2015 *Phys. Rev. Lett.* **115** 216806
[31] Chaudhary S, Lewandowski C, and Refael G 2021 arXiv:2107.09090
[32] Wang H, Tang X Y, Xu H W, Li J, and Qian X F 2022 *npj Quantum Mater.* **7** 61
[33] Resta R 2024 *Phys. Rev. Lett.* **133** 206903
[34] Ahn J Y, Guo G Y, and Nagaosa N 2020 *Phys. Rev. X* **10** 041041
[35] De Juan F, Grushin A G, Morimoto T, and Moore J E 2017 *Nat. Commun.* **8** 15995
[36] Qian C, Yu C, Jiang S C, Zhang T, Gao J C, Shi S, Pi H Q, Weng H M, and Lu R F 2022 *Phys. Rev. X* **12** 021030
[37] Sivianes J and Ibañez-Azpiroz J 2023 *Phys. Rev. B* **108** 155419
[38] Gao Y, Yang S Y A, and Niu Q 2014 *Phys. Rev. Lett.* **112** 166601
[39] Neufeld O, Tancogne-Dejean N, Hübener H, De Giovannini U, and Rubio A 2023 *Phys. Rev. X* **13** 031011
[40] Schüler M, De Giovannini U, Hübener H, Rubio A, Sentef M A, and Werner P 2020 *Sci. Adv.* **6** eaay2730
[41] Wu D Z, Ye M, Chen H W, Xu Y, and Duan W H 2024 *npj Comput. Mater.* **10** 79
[42] Wang J Z, Ye M, Guo X M, Li Y, Zou N L, Li H, Zhang Z T, Zhao S B, Xu Z M, Chen H W, Wu D Z, Bao T, Xu Y, and Duan W H 2024 *Phys. Rev. Mater.* **8** 085202
[43] Wang Y R, Tokman M, and Belyanin A 2016 *Phys. Rev. B* **94** 195442
[44] Xiao D, Chang M C, and Niu Q 2010 *Rev. Mod. Phys.* **82** 1959
[45] Wang H and Chang K 2024 arXiv:2405.13355
[46] Hu J M, Li W B, Wang H, and Chang K 2024 arXiv:2410.09677
[47] Kaplan D, Holder T, and Yan B H 2023 *Nat. Commun.* **14** 3053
[48] Kaplan D, Holder T, and Yan B H 2024 *Phys. Rev. Lett.* **132** 026301
[49] Chen H W, Ye M, Zou N L, Gu B L, Xu Y, and Duan W H 2022 *Phys. Rev. B* **105** 075123
[50] Parker D E, Morimoto T, Orenstein J, and Moore J E 2019 *Phys. Rev. B* **99** 045121
[51] Holder T, Kaplan D, and Yan B H 2020 *Phys. Rev. Res.* **2** 033100
[52] Ventura G B, Passos D J, Lopes dos Santos J M B, Viana Parente Lopes J M, and Peres N M R 2017 *Phys. Rev. B* **96** 035431
[53] Passos D J, Ventura G B, Viana Parente Lopes J M, Lopes dos Santos J M B, and Peres N M R 2018 *Phys. Rev. B* **97** 235446
[54] Ma Q, Xu S Y, Shen H T, MacNeill D, Fatemi V, Chang T R, Mier Valdivia A M, Wu S F, Du Z Z, Hsu C H, Fang S A, Gibson Q D, Watanabe K, Taniguchi T, Cava R J, Kaxiras E, Lu H Z, Lin H, Fu L, Gedik N, and Jarillo-Herrero P 2019 *Nature* **565** 337
[55] Wang N Z, Kaplan D, Zhang Z W, Holder T, Cao N, Wang A F, Zhou X Y, Zhou F G, Jiang Z Z, Zhang C S, Ru S H, Cai H B, Watanabe K, Taniguchi T, Yan B H, and Gao W B 2023 *Nature* **621** 487
[56] Gao A Y, Liu Y F, Qiu J X, Ghosh B, Trevisan T V, Onishi Y, Hu C W, Qian T M, Tien H J, Chen S W, Huang M Q, Bérubé D, Li H C, Tzschaschel C, Dinh T, Sun Z, Ho S C, Lien S W, Singh B, Watanabe K, Taniguchi T, Bell D C, Lin H, Chang T R, Du C R, Bansil A, Fu L, Ni N, Orth P P, Ma Q, and Xu S Y 2023 *Science* **381** 181
[57] Shi L K, Matsyshyn O, Song J C W, and Villadiego I S 2023 *Phys. Rev. B* **107** 125151
[58] Matsyshyn O, Song J C W, Villadiego I S, and Shi L K 2023 *Phys. Rev. B* **107** 195135
[59] Onishi Y, Watanabe H, Morimoto T, and Nagaosa N 2022 *Phys. Rev. B* **106** 235110
[60] Kaplan D, Holder T, and Yan B H 2020 *Phys. Rev. Lett.* **125** 227401
[61] Keldysh L V 1965 *Sov. Phys. JETP* **20** 1307
[62] Vampa G, McDonald C R, Orlando G, Klug D D, Corkum P B, and Brabec T 2014 *Phys. Rev. Lett.* **113** 073901
[63] Vampa G, McDonald C R, Orlando G, Corkum P B, and Brabec T 2015 *Phys. Rev. B* **91** 064302
[64] Yue L and Gaarde M B 2020 *Phys. Rev. Lett.* **124** 153204
[65] Chacón A, Kim D, Zhu W, Kelly S P, Dauphin A, Pisanty E, Maxwell A S, Picón A, Ciappina M F, Kim D E, Ticknor C, Saxena A, and Lewenstein M 2020 *Phys. Rev. B* **102** 134115
[66] Yue L and Gaarde M B 2023 *Phys. Rev. Lett.* **130** 166903
[67] Haldane F D M 1988 *Phys. Rev. Lett.* **61** 2015
[68] Hasan M Z and Kane C L 2010 *Rev. Mod. Phys.* **82** 3045
[69] Ding K, Fang C, and Ma G C 2022 *Nat. Rev. Phys.* **4** 745
[70] Zhang K, Fang C, and Yang Z S 2023 *Phys. Rev. Lett.* **131** 036402
[71] Zhang K, Yang Z S, and Fang C 2020 *Phys. Rev. Lett.* **125** 126402
[72] Hu S Q, Zhao H, Liu X B, Chen Q, Chen D Q, Zhang X Y, and Meng S 2024 *Phys. Rev. Lett.* **133** 156901
[73] Mao W W, Rubio A, and Sato S A 2022 *Phys. Rev. B* **106** 024313
[74] See Supplemental Material at URL for detailed formulation in Keldysh approach, computational details of numerical calculations and symmetry analysis in standard Haldane model, symmetry criteria for quantum geometric tensor contribution in SHG susceptibility, SHG susceptibility during topological phase transition, impact of relaxation and experimental detection including Refs. [7,17,18,29,30,61–66,85,87,88].
[75] Ahn J Y, Guo G Y, Nagaosa N, and Vishwanath A 2022 *Nat. Phys.* **18** 290
[76] Rensink T C and Antonsen T M 2016 *Phys. Rev. A* **94** 063407
[77] Esteve-Paredes J J and Palacios J J 2023 *SciPost Phys. Core* **6** 002
[78] Gallego S V, Etxebarria J, Elcoro L, Tasci E S, and Perez-Mato J M 2019 *Acta Crystallogr. Sect. A* **75** 438
[79] Li L, Lan P F, Zhu X S, and Lu P X 2023 *Rep. Prog. Phys.* **86** 116401
[80] Allen R E 1979 *Phys. Rev. B* **19** 917
[81] Yokomizo K and Murakami S 2019 *Phys. Rev. Lett.* **123** 066404
[82] Longhi S 2021 *Phys. Rev. B* **104** 125109
[83] Liu L, Liu W K, Cheng B, Cui B, and Hu J F 2023 *J. Phys. Chem. Lett.* **14** 370
[84] Wang S X, Zhang Z C, Li H Y, Sanborn C, Zhao W Y, Wang S Q, Watanabe K, Taniguchi T, Crommie M F, Chen G R, and Wang F 2024 *Nano Lett.* **24** 6838
[85] Knippels G M H, Meer A F G, MacLeod A M, Yelisseyev A, Isaenko L, Lobanov S, Thénot I, and Zondy J J 2001 *Opt. Lett.* **26** 617
[86] Ruan Y P, Tang J S, Li Z P, Wu H D, Zhou W P, Xiao L Q, Chen J F, Ge S J, Hu W, Zhang H, Qiu C W, Liu W M, Jing H, Lu Y Q, and Xia K Y 2024 *Nat. Photon.* **19** 109
[87] Luther J M, Jain P K, Ewers T, and Alivisatos A P 2011 *Nat. Mater.* **10** 361
[88] Jiang J, Saito R, Grüneis A, Dresselhaus G, and Dresselhaus M S 2004 *Chem. Phys. Lett.* **392** 383